Reduction of dental filling metallic artifacts in CT-based attenuation correction of PET data using weighted virtual sinograms optimized by a genetic algorithm

Mehrsima Abdoli
Department of Nuclear Medicine and Molecular Imaging, University Medical Center Groningen, University of Groningen, 9700 RB Groningen, The Netherlands

Mohammad Reza Ay
Department of Medical Physics and Biomedical Engineering, School of Medicine, Tehran University of Medical Sciences, Tehran, Iran; Research Center for Science and Technology in Medicine, Tehran University of Medical Sciences, Tehran, Iran; and Research Institute for Nuclear Medicine, Tehran University of Medical Sciences, Tehran, Iran

Alireza Ahmadian
Department of Medical Physics and Biomedical Engineering, School of Medicine, Tehran University of Medical Sciences, Tehran, Iran and Research Center for Science and Technology in Medicine, Tehran University of Medical Sciences, Tehran, Iran

Rudi A. J. O. Dierckx
Department of Nuclear Medicine and Molecular Imaging, University Medical Center Groningen, University of Groningen, 9700 RB Groningen, The Netherlands

Habib Zaidi[a)]
Division of Nuclear Medicine, Geneva University Hospital, CH-1211 Geneva, Switzerland; Geneva Neuroscience Center, Geneva University, CH-1211 Geneva, Switzerland; and Department of Nuclear Medicine and Molecular Imaging, University Medical Center Groningen, University of Groningen, Groningen, The Netherlands

(Received 5 July 2010; revised 23 September 2010; accepted for publication 6 October 2010; published 8 November 2010)

Purpose: The presence of metallic dental fillings is prevalent in head and neck PET/CT imaging and generates bright and dark streaking artifacts in reconstructed CT images. The resulting artifacts would propagate to the corresponding PET images following CT-based attenuation correction (CTAC). This would cause over- and/or underestimation of tracer uptake in corresponding regions thus leading to inaccurate quantification of tracer uptake. The purpose of this study is to improve our recently proposed metal artifact reduction (MAR) approach and to assess its performance in a clinical setting.

Methods: The proposed MAR algorithm is performed in the virtual sinogram space to overcome the challenges associated with manipulating raw CT data. The corresponding bins of the virtual sinogram affected by metallic objects are obtained by forward projection of segmented metallic objects in the original CT image. These bins are then substituted by weighted values of three estimates: the affected bins in the original sinogram, the bins in the corrected sinogram using spline interpolation, and the sinogram bins in the neighboring column of the sinogram matrix. The optimized weighting factors (α, β, and γ) were estimated using a genetic algorithm (GA). The optimized combination of weighting coefficients was obtained using the GA applied to 24 clinical CT data sets. The proposed MAR method was then applied to 12 clinical head and neck PET/CT data sets containing dental artifacts. Analysis of the results was performed using Bland and Altman plots and a method allowing analysis in the absence of gold standard called regression without truth (RWT). The proposed method was also compared to an image-based MAR method.

Results: Optimization of the weighting coefficients using the GA resulted in an optimum combination of parameters of α=0.26, β=0.67, and γ=0.07. According to Bland and Altman plots generated for both CT and PET images of the clinical data, the proposed MAR algorithm is efficient for reduction of streak artifacts in CT images and such reduce the over- and/or underestimation of tracer uptake. The RWT method also confirmed the effectiveness of the proposed MAR method. The obtained figures of merit revealed that attenuation corrected PET data corrected using CTAC after applying the MAR algorithm are more similar to the assumed gold standard. Comparison with the knowledge-based method revealed that the proposed method mainly corrects the artifactual

regions without modifying the unaffected regions. The knowledge-based method globally modifies the images including those that do not include metallic artifacts.
Conclusions: The proposed MAR algorithm improves the quality and quantitative accuracy of clinical head and neck PET/CT images and could be easily integrated in clinical setting. © *2010 American Association of Physicists in Medicine*. [DOI: 10.1118/1.3511507]

Key words: PET/CT, attenuation correction, metal artifacts, virtual sinogram, genetic algorithm

I. INTRODUCTION

The deployment of combined PET/CT scanners is considered as one of the growing technological advances which fulfils the drawbacks of using two separate imaging modalities.[1] The alignment of anatomical and functional images achieved by hardware-based image registration has improved the capabilities of PET/CT for clinical diagnosis, assessment of response to therapy, surgery and treatment planning, and prognosis assessment.[2] Another advantageous characteristic of PET/CT systems is that CT numbers or Hounsfield units (HUs) reflect the attenuation properties of the tissues. Consequently, CT images can be utilized for attenuation correction (AC) of the corresponding PET data. This requires a reliable conversion procedure for generating an attenuation map (μmap) from CT images, which comprises three main steps: downsampling, energy mapping, and smoothing. Downsampling must be performed to make the voxel sizes of CT and PET images identical. Since the linear attenuation coefficients (LACs) measured by CT is calculated at the x-ray effective energy rather than at 511 keV, energy mapping involves the conversion of LACs at CT energies to those corresponding to 511 keV. Considering that the spatial resolution of PET images is worse than that of CT images, the last step consists of smoothing CT images to match the spatial resolution of the corresponding PET data.[3,4]

One should, however, be aware of the extra effort needed to handle potential sources of error and artifact impacting the quality of CT images which can propagate to PET images during the CT-based attenuation correction (CTAC) process. The presence of highly attenuating objects (having a high atomic number) is considered as one of the strongest sources of artifact which generate dark and bright streaks in the reconstructed CT images. These streaks, called metallic artifacts, are produced owing to beam hardening effect as an insufficient number of photons will reach the detectors. This type of artifacts is induced by metallic implants such as surgical clips, hip prosthesis, and dental fillings which cause an inconsistency in reconstructed CT images. As a result, the generated μmap does not reflect actual attenuation coefficients in the regions corresponding to streak artifacts. This can lead to inaccurate quantification of tracer uptake in the corresponding regions of PET images.[5–7] Although it was reported that the visual quality of attenuation corrected PET images is not affected to a great extent by poorly visible artifacts,[8] it should be emphasized that quantification is one of the strengths of PET compared with other modalities since it generates quantitative images of regional tracer uptake that are linked to the underlying physiologic or pharmacokinetic processes occurring in the organs/tissues of interest. The accurate quantification of PET data can only be achieved when different sources of error and artifact are corrected for. This issue remains controversial and requires further investigation.

In order to obtain a reliable μmap for accurate CTAC of PET data, metal artifact reduction (MAR) in CT images is imperative. This challenging issue was addressed using several techniques.[3] In general, MAR methods can be classified into two main categories: sinogram- and image-based methods. Sinogram-based methods implement the correction procedure in the sinogram space. Different techniques belonging to this category have been proposed; linear interpolation of the missing sinogram bins being one of them.[9,10] In this method, metallic objects are first segmented using a simple thresholding technique. The segmented image is then forward projected to identify the sinogram bins affected by metallic objects. The affected sinogram bins are then substituted by those derived from linear interpolation of adjacent sinogram bins along the same projection angle. The inverse Radon transform using the filtered backprojection algorithm is the final step to reconstruct the interpolated sinogram and obtain the corrected CT image. Another approach belonging to this category of methods is cubic spline interpolation of unaffected sinogram bins.[11] Another way of replacing the affected projection data is substitution by the unaffected corresponding projections.[12] This method replaces the missing projections by unaffected projections in the opposite angular position in spiral scanning or in the same angular position of the next slice in step scanning.

Image-based MAR methods manipulate the reconstructed images rather than the corresponding raw CT data. Techniques belonging to this category include iterative deblurring,[13] methods using wavelets,[14,15] knowledge-based techniques,[16] segmentation,[17] and pattern recognition-based techniques.[18] This category of MAR methods uses different enhancement approaches to remove the artifacts considered as unwanted objects. The intrinsic obscurity between CT numbers corresponding to artifactual regions and surrounding tissues strongly affects the precision of the enhancement procedure owing to the intricacy of detecting regions affected by metallic artifacts.

Although sinogram-based methods are capable of obtaining more accurate results,[19] the major challenge facing their practical implementation is the requirement to handle large raw CT data usually stored in encrypted manufacturer-dependent proprietary format. The objective of this study is to utilize an easy to use virtual sinogram method as an alternative and to improve its performance using a genetic

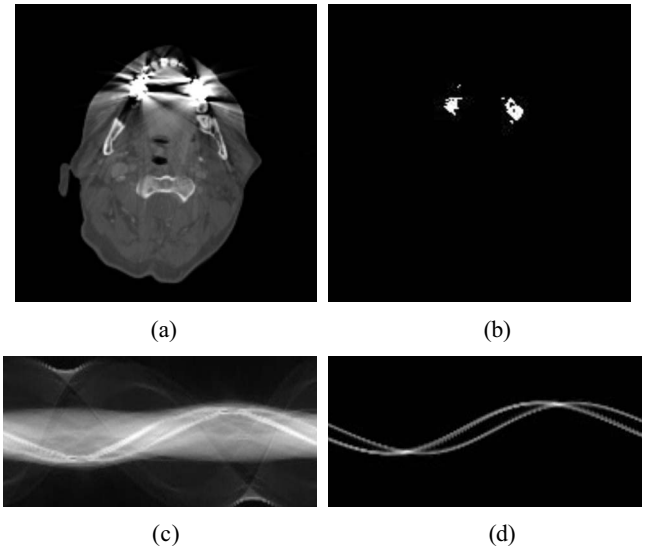

FIG. 1. Detection of projections affected by metallic objects: (a) original CT image, (b) thresholded image, (c) original sinogram, and (d) metal-only sinogram.

algorithm-based approach for reduction of dental metallic artifacts in clinical head and neck PET/CT imaging.

II. MATERIALS AND METHODS

II.A. MAR algorithm

To overcome the above mentioned limitations of using the original CT raw data, the proposed method utilizes the concept of virtual sinogram as an alternative to benefit from the advantages of sinogram-based MAR methods.[20] A virtual sinogram is obtained by 2D forward projection of the reconstructed CT image. The sinogram matrix dimension depends on the definition of the x-ray tube and detector geometry and the projection parameters which are set according to the scanner specifications.

The MAR procedure starts by segmenting metallic objects causing the bright and dark regions in the reconstructed CT image so that the projection data affected by these objects can be detected in the sinogram space. This is performed by automated global thresholding of CT images since the HUs related to metallic objects are considerably higher than those associated with other biological tissues. This approach might result in extracting few pixels associated with metallic artifacts containing very strong artifacts. However, this effect has a negligible influence on the final corrected images and as such a more complicated metal extraction method is not required. By assigning a nil value to other regions of the image, a thresholded image can be extracted [Figs. 1(a) and 1(b)]. To identify the affected projection data, the thresholded image is forward projected using the same geometry and projection parameters. The resulting sinogram contains some bins with a nil value that represent the projection data which are not affected by metallic objects. It also contains some bins having a value greater than zero, representing the affected projection data, which need to be replaced by appropriate values [Figs. 1(c) and 1(d)].

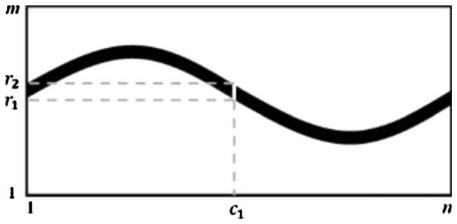

FIG. 2. Schematic view of a sinogram. This sinogram is a $m \times n$ matrix where r denotes the rows and c denotes the columns. The sinus-shape part represents the interpolated sinogram bins. The improvement scheme for each column (e.g., c_1) is applied on the interpolated sinogram bins (i.e., the pixels in rows r_1 to r_2 and in column c_1. It must be noted that only the sinogram bins affected by metallic objects are shown to simplify the diagram. The bins associated with other objects are not illustrated.

The replacement scheme follows a spline interpolation technique to estimate the values of affected bins in each column of the sinogram matrix according to those of neighboring unaffected bins in the same column. The spline method was chosen owing to its capability to join discontinuous data by fitting an appropriate polynomial curve to the whole set.[21] Although the use of the spline interpolation technique results in the smoothest replacing values in the interpolated sinogram, the sinogram suffers from discontinuity along the second dimension of the matrix since the interpolation is applied in one dimension of the sinogram matrix (i.e., along the matrix columns). Moreover, since the shape of the metallic object is not necessarily symmetric, in some projection angles, the x-ray projections traverse a cross section of the metallic object with larger size, leading to a higher number of missing projections. This results in a higher number of replaced bins in a single column of the sinogram matrix. In such cases, the estimates of interpolated bins have an obvious difference with the neighboring unaffected bins in the same column due to the inefficiency of the interpolation technique when used for a large number of missing data. Consequently, the interpolated sinogram needs improvement before it can be used for reconstruction of the corrected image.

This is achieved by assigning a fraction of three different projection data to generate the corrected sinograms. The involved data sets include the influenced bins in the interpolated and uncorrected sinograms, as well as the neighboring column of the sinogram matrix. The assignment procedure has to be started from a column in the sinogram matrix in which the difference between the interpolated and unaffected bins is minimal. Such a column, referred to as c_o, is considered as starting point of the improvement procedure. The differences between the interpolated and unaffected bins can be calculated using Eq. (1) which estimates the mean difference between the interpolated and unaffected bins in each column (c). In a sinogram matrix (S) which has dimension of $m \times n$, the interpolated bins pertaining to a single metallic object form a sinuslike shape similar to what is presented in Fig. 2. Consequently, the mean difference equation for each column $c \in [1, n]$ can be written in the following form:

$$\varepsilon(c)=\frac{\left|S(r_1-1,c)-\frac{\sum_{i=r_1}^{r_2}S(i,c)}{r_2-r_1+1}\right|+\left|S(r_2+1,c)-\frac{\sum_{i=r_1}^{r_2}S(i,c)}{r_2-r_1+1}\right|}{2}, \tag{1}$$

where ε is the mean difference of interpolated sinogram bins and unaffected bins in the same column and r_1 and r_2 indicate the range of rows ($[r_1,r_2]$) representing missed sinogram bins in each column. Figure 2 shows schematically the situation for a specific column $c=c_1$. It can be seen that the values of r_1 and r_2 will change for different columns since they represent the position of the missed sinogram bins in each column.

When ε is calculated for all columns, the column associated with the lowest mean difference will be considered as the starting point of the improvement procedure. After the starting point is determined, the final intensity of the bins is estimated using the first part of Eq. (2) for columns located on the right side of this point and using the second part of the same equation for columns located on the left side. In other words, when the columns on the right side of the starting point are being improved, the column on the left will be considered as the neighboring column and will have a proportion in the final improved sinogram. Likewise, when improving the columns on the left side of the starting point, the column on the right side will be considered as the neighboring column,

$$S_{\text{improved}}(r,c)=\begin{cases}\alpha S_{\text{main}}(r,c)+\beta S_{\text{interpolated}}(r,c)+\gamma\dfrac{\sum_{i=r_1}^{r_2}S_{\text{improved}}(i,c-1)}{r_2-r_1+1} & c>c_o\\ \alpha S_{\text{main}}(r,c)+\beta S_{\text{interpolated}}(r,c)+\gamma\dfrac{\sum_{i=r_1}^{r_2}S_{\text{improved}}(i,c+1)}{r_2-r_1+1} & c<c_o,\end{cases} \tag{2}$$

where S_{improved} is the improved sinogram, S_{main} is the uncorrected sinogram, $S_{\text{interpolated}}$ is the corrected sinogram using our method,[20] r and c represent the rows and columns of the sinogram matrices, r_1 and r_2 are the lowest and highest affected rows in each column, and α, β, and γ are the weighting factors assigned to S_{main}, $S_{\text{interpolated}}$, and S_{improved}, respectively.

In a previous work we examined different combinations of the weighting factors α, β, and γ having values in the range of [0.1–0.9] to find the optimal combination.[22] Thereafter, the best combination was selected based on visual assessment and statistical analysis of the resulting μmaps. This approach was restrictive in the sense that only a limited set of combinations were investigated. Moreover, visual assessment is prone to error owing to its subjective nature. As a result, the use of fully automated optimization methods to select the optimal combination of weighting factors among a wider range of values is commended. A genetic algorithm was used to achieve this goal.

After finding the optimal set of weighting coefficients, the improved sinogram is calculated using Eq. (2) and the corrected CT images generated by reconstructing the corrected sinograms. A filtered backprojection MATLAB routine is applied for reconstruction of artifact-free images. The geometry of the x-ray tube and detectors and the projection parameters were similar to those used by the forward projection procedure.

II.B. Genetic algorithm

Genetic algorithms (GAs) are computerized optimization methods which operate on the basis of natural evolution. They select a set of solutions, called chromosomes or genomes as variables of a function, referred to as the fitness function. This set of solutions is considered as an initial population which is used to create new generations iteratively. The new generations are produced according to mutation and crossover operations between the individuals of the population.[23] GAs try to find the best and fittest set of solutions for each function.

The GA's function is dependent on how the fitness function is defined and how the algorithm is terminated or limited. In the present work, the fitness function was defined as the mean difference between a region associated with metallic artifacts defined on the corrected CT image and the corresponding region in an adjacent artifact-free slice. Such corresponding slices do not necessarily exist in all clinical

studies; therefore a number of data sets satisfying this criterion were carefully selected for this purpose. This mean difference is expected to be minimal. Therefore, the role of the GA is to examine different combinations of the weighting factors (α, β, and γ) and to find a unique combination minimizing the fitness function. The limitation criterion is the range of values which can be assigned to the weighting coefficients. Since these coefficients represent a proportion of each data set that is going to be incorporated into the final data, their value is usually between 0 and 1. Also the summation of all weighting factors must result in a 100% proportion, i.e.,

$$\alpha+\beta+\gamma=1, \quad 0<\alpha,\beta,\gamma<1.$$

II.C. Clinical studies

Two groups of clinical data sets were utilized: the first aimed to establish the method by obtaining the optimum values of the weighting coefficients α, β, and γ (method-establishing data sets), whereas the second was used to evaluate the performance of the method (method-testing data sets). The GA was applied on the method-establishing data sets which include 24 clinical CT images obtained on a clinical GE LightSpeed VCT 64 slice x-ray CT scanner (General Electric Healthcare Technologies, Waukesha, WI), whereas the improved MAR method was applied on the method-testing data sets containing 12 clinical PET/CT data sets obtained from a Biograph 16-slice PET/CT scanner (Siemens Medical Solutions, Erlangen, Germany). The PET/CT data acquisition was performed using a standard protocol recommended by the manufacturer. The PET data acquisition was started approximately 60 min after injection of 370 MBq of [^{18}F]-FDG, 3 min per bed position. CT data acquisition was performed under standard conditions (120 kVp, 180 mAs, 16×1.5 collimation, a pitch of 1.2, and 1 s per rotation). PET image reconstruction was performed using attenuation-weighted, ordered subset-expectation maximization (AW-OSEM) iterative reconstruction algorithm. The reconstruction parameters were set to the default values (four iterations, eight subsets, and a postprocessing Gaussian kernel with a FWHM of 5 mm).

II.D. Data analysis

Each method-testing data set includes a number of slices containing dental metallic artifacts. In each slice of uncorrected CT images, five identical regions of interest (ROIs) were manually defined, two of which were located in the overestimated regions, two in the underestimated regions, and one in the unaffected region. The same regions were defined on the corresponding corrected CT images, as well as the PET images corrected for attenuation using both uncorrected and MAR corrected CT images. Bland–Altman plots were utilized to compare the mean values of the defined ROIs in both CT and PET images and to assess the agreement between them.

The method-testing clinical data sets were also analyzed using the regression without truth (RWT) technique proposed by Hoppin *et al.*[24] This method is used to compare the magnitude of a parameter resulting from the use of different modalities when the gold standard is not known. In the present work, this method can be used to compare the intensity values of reconstructed PET data (in terms of Bq/cc) corrected by the original and MAR corrected CT data. In RWT, it is assumed that there is a linear relationship between the true value of the parameter for a given patient Θ_p and the corresponding estimated value by a given modality θ_{pm}. This linear relationship can be written in the following form:

$$\theta_{pm}=a_m\Theta_p+b_m+\varepsilon_{pm}, \tag{3}$$

where a_m and b_m are the slope and intercept of the patient-independent linear model characterizing the modality. ε_{pm} represents the noise term having a normal distribution with zero mean and variance of σ_m^2. It should also be assumed that Θ_p is constant for a given patient in all modalities and is statistically independent from patient to patient.

According to this method, a figure of merit (FOM) can be defined using the linear model parameters to evaluate the performance of modalities as follows:

$$\gamma_m=\sigma_m/a_m. \tag{4}$$

Suppose that we acquired PET data for P patients corrected using two CT data sets: the first data set is not corrected for dental metallic artifacts, whereas the second is corrected using the proposed MAR algorithm. Therefore, these two data sets can be considered as the two modalities which are going to be compared to each other. The estimated values for each modality θ_{pm} can be calculated from the resulting images. The method calculates the log-likelihood of the true value using Eq. (3) and the prementioned assumptions,

$$\lambda=P\ln\left(\prod_{m=1}^{M}\frac{1}{\sqrt{2\pi\sigma_m^2}}\right)+\sum_{p=1}^{P}\ln\left[\int d\Theta_p pr(\Theta_p)\times\exp\left(\sum_{m=1}^{M}\left(-\frac{1}{2\sigma_m^2}(\theta_{pm}-a_m\Theta_p-b_m)^2\right)\right)\right], \tag{5}$$

where P is the total number of patients and M the number of modalities to be compared ($M=2$ in our case). It can be observed from this equation that although the true value is not required in the log-likelihood calculations, an approximate knowledge of the distribution of true values $pr(\Theta_p)$ is required. Since in most cases the exact distribution of the true values is unknown, an assumed distribution can be applied to obtain estimates of the linear model parameters. We evaluated a number of clinical PET data without any dental metallic implants and explored the distribution of voxel intensities in the region of head and neck excluding the brain. The overall distribution closely looks like a truncated normal distribution. As a result, the truncated normal distribution was selected as distribution of the true values. Applying the truncated normal distribution form to Eq. (5) and considering two modalities, we obtain

$$\lambda = P\ln(\sigma_1\sigma_2) + \sum_{p=1}^{P}\left(\frac{\beta^2-4\alpha\gamma}{4\alpha}\right)\cdot\ln\left(\frac{1}{2\sqrt{2\pi\sigma^2}}\sqrt{\frac{\pi}{\alpha}}\left[\operatorname{erf}\left(\frac{2\alpha+\beta}{2\sqrt{\alpha}}\right)-\operatorname{erf}\left(\frac{\beta}{2\sqrt{\alpha}}\right)\right]\right)+\text{constant}, \quad (6)$$

where

$$\alpha = \frac{1}{2\sigma^2}+\frac{a_1^2}{2\sigma_1^2}+\frac{a_2^2}{2\sigma_2^2},$$

$$\beta = -\frac{\mu}{\sigma^2}-\frac{a_1(\theta_{p1}-b_1)}{\sigma_1^2}-\frac{a_2(\theta_{p2}-b_2)}{\sigma_2^2},$$

$$\gamma = \frac{\mu^2}{2\sigma^2}+\frac{(\theta_{p1}-b_1)^2}{2\sigma_1^2}+\frac{(\theta_{p2}-b_2)^2}{2\sigma_2^2},$$

and erf denotes the "error function" having a special of sigmoid shape defined as

$$\operatorname{erf}(x) = \frac{2}{\sqrt{\pi}}\int_0^x e^{-t^2}dt. \quad (7)$$

The parameters of the linear model a_m, b_m, and σ_m can be estimated by maximizing the log-likelihood λ. The model parameters were calculated using five ROIs defined on the regions affected by artifacts in both original and corrected images. For the purpose of maximizing the log-likelihood as a function of the model parameters, a quasi-Newton optimization method was utilized. Thereafter, the FOM for each modality was calculated to evaluate the performance of each modality.

The results of the proposed MAR algorithm were also compared with those obtained using an image-based MAR technique referred to as knowledge-based method originally proposed by Hamill *et al.*[16] and implemented on vendor supplied software (Syngo Multimodality Workplace, Siemens Medical Solutions, Erlangen, Germany). Two clinical head and neck PET/CT cases with dental implants were used for this purpose.

III. RESULTS

As stated earlier, the optimization of weighting coefficients using the genetic algorithm was applied to 24 clinical head and neck CT images containing metallic dental fillings (method-establishing data sets). The result of the optimization procedure is given in Table I. The mean value of the obtained weighting factors is considered as the optimal proportions of the original sinogram, interpolated sinogram, and the neighboring columns, respectively. The rounded optimal values of the weighting factors are α=0.26, β=0.67, and γ=0.07. The improvement brought to the method through the use of optimized weighting factors is illustrated in Fig. 3. As can be observed in the inserts of Figs. 3(b) and 3(c), the discontinuities and differences between the interpolated and unaffected projection data have been reduced.

TABLE I. Weighting coefficients (α, β, and γ) obtained using the genetic algorithm optimization method calculated from 24 clinical CT images containing metallic dental fillings.

	Weighting coefficients		
Patient number	α	β	γ
1	0.30	0.57	0.13
2	0.31	0.58	0.11
3	0.36	0.50	0.14
4	0.44	0.51	0.05
5	0.38	0.52	0.10
6	0.17	0.71	0.12
7	0.26	0.74	0.00
8	0.35	0.53	0.12
9	0.15	0.85	0.00
10	0.37	0.59	0.04
11	0.09	0.86	0.05
12	0.27	0.72	0.01
13	0.30	0.68	0.02
14	0.39	0.60	0.01
15	0.22	0.59	0.19
16	0.24	0.64	0.12
17	0.24	0.73	0.03
18	0.10	0.84	0.06
19	0.24	0.74	0.02
20	0.18	0.78	0.04
21	0.36	0.51	0.13
22	0.30	0.64	0.06
23	0.20	0.72	0.08
24	0.12	0.85	0.03
mean	0.26	0.67	0.07
SD	0.10	0.12	0.05

The proposed MAR algorithm is also applied to 12 clinical head and neck PET/CT studies (method-testing data sets). Figures 4 and 5 show the influence of the method on both CT and PET images of two patient studies. It can be seen that the proposed MAR algorithm reduces to a considerable extent the over/underestimation of attenuation coefficients in some regions of CT images. Likewise, its impact on the corrected PET images is clearly visible on the subtraction images [Figs. 4(e) and 5(e)].

As expected, the subtraction image has high positive values in areas corresponding to bright regions in CT images. Likewise, the subtracted image has negative values in re-

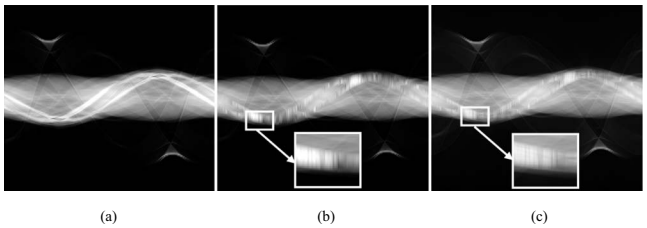

FIG. 3. Sinograms of the CT image of a clinical study showing: (a) uncorrected sinogram, (b) sinogram corrected using the previously reported virtual sinogram method (before improvement), and (c) sinogram corrected using the improved virtual sinogram method. Note the continuity of the corrected sinogram shown in (c).

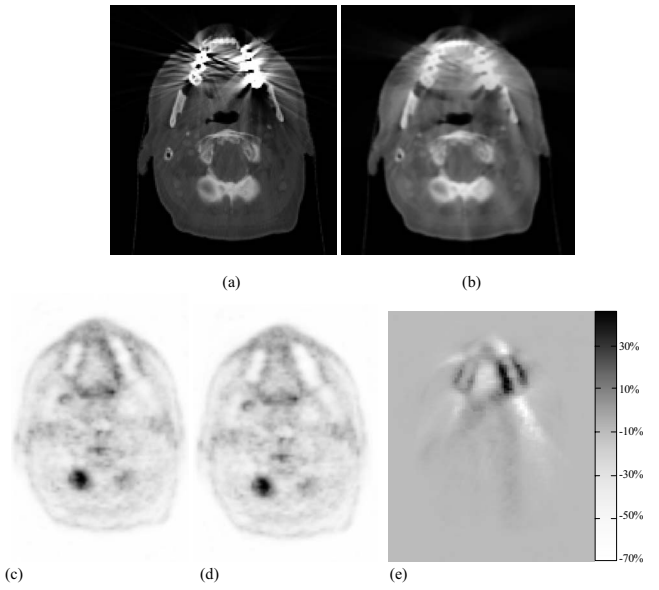

FIG. 4. Clinical CT images of one clinical study reconstructed using the (a) uncorrected and (b) corrected virtual sinograms. [(c) and (d)] The corresponding attenuation corrected PET images and (e) subtraction of images shown in (c) and (d).

gions corresponding to dark regions in CT images, Bland–Altman plots were used to illustrate the differences between uncorrected and corrected CT and PET data. Figures 6 and 7 show the results of this analysis. All the slices in each data set containing dental metallic artifacts are considered in these plots. Each data set is represented by a distinct symbol for clarity. The overestimated, underestimated, and unaffected regions in each data set are also identified in red, blue, and green, respectively. The plots for both CT and PET images confirm that the intensities of the artifactual regions are modified in the desired manner after applying the proposed MAR algorithm (i.e., the intensities of the over- and underestimated regions are reduced and increased, respectively), whereas the intensities of the unaffected regions remain almost similar.

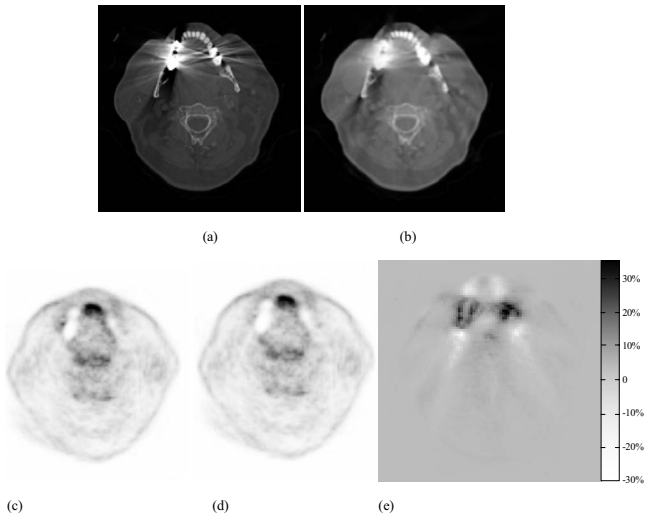

FIG. 5. Clinical CT images of another clinical study reconstructed using the (a) uncorrected and (b) corrected virtual sinograms. [(c) and (d)] The corresponding attenuation corrected PET images and (e) subtraction of images shown in (c) and (d).

Data analysis using Hoppin's method revealed that the corrected PET data sets using the proposed MAR algorithm are more similar to the assumed gold standard. The obtained FOM corresponding to the PET images corrected using the uncorrected CT images is 0.16, whereas the one corresponding to PET images corrected by the MAR corrected CT images is 0.10. The FOM of the PET data corrected by the proposed MAR algorithm is lower than the one obtained using PET data corrected for attenuation using the uncorrected CT data. Therefore, the corrected PET images are more similar to the ground truth (gold standard).

The head and neck PET data were reconstructed three times using different attenuation maps: first using CT data not corrected for metallic artifacts, second using the proposed MAR algorithm, and finally using the MAR method proposed by Hamill *et al.*[16] Figures 8 and 9 illustrate the results of the three reconstructions as well as the subtraction of PET images obtained using the two MAR methods. As can be observed, both methods reduce the artifacts visible in both over- and underestimated regions. However, the method by Hamill *et al.*[16] results in larger modifications of the activity concentrations in over- and underestimated regions compared to the proposed MAR algorithm.

To illustrate the impact of the two MAR algorithms on CT data free of metallic artifacts, Fig. 10 shows one of the slices of the first clinical case where the difference between the two MAR methods in the absence of metallic objects is put forward through the subtraction of the resulting images from the one obtained without application of MAR.

IV. DISCUSSION

Dental metallic artifacts have proven to be one of the strongest sources of artifact resulting from the CTAC procedure.[5,6] Therefore, significant effort has been made in the last few years to assess its clinical relevance. The visual effect of minor artifacts which are not strong enough to get propagated to attenuation corrected PET images has proven to be clinically insignificant.[8] However, the errors and artifacts visible in CT images need to be minimized to reduce the bias and achieve more accurate quantification of PET data. Hence, application of an appropriate MAR method prior to CTAC procedure is highly desired.

In the proposed MAR algorithm the projection bins affected by metallic objects are first substituted using a spline interpolation scheme. Subsequently, the interpolated virtual sinogram is improved using weighting factors assigned to three different data sets: the influenced bins in the original sinogram, the bins in the corrected sinogram using spline interpolation, and values of the sinogram bins in the neighboring column of the sinogram matrix. A segment of the LOR crossing the metallic object contains incorrect data, whereas the remaining segment crossing other biological tissues contains correct data. Incorporating a weighted propor-

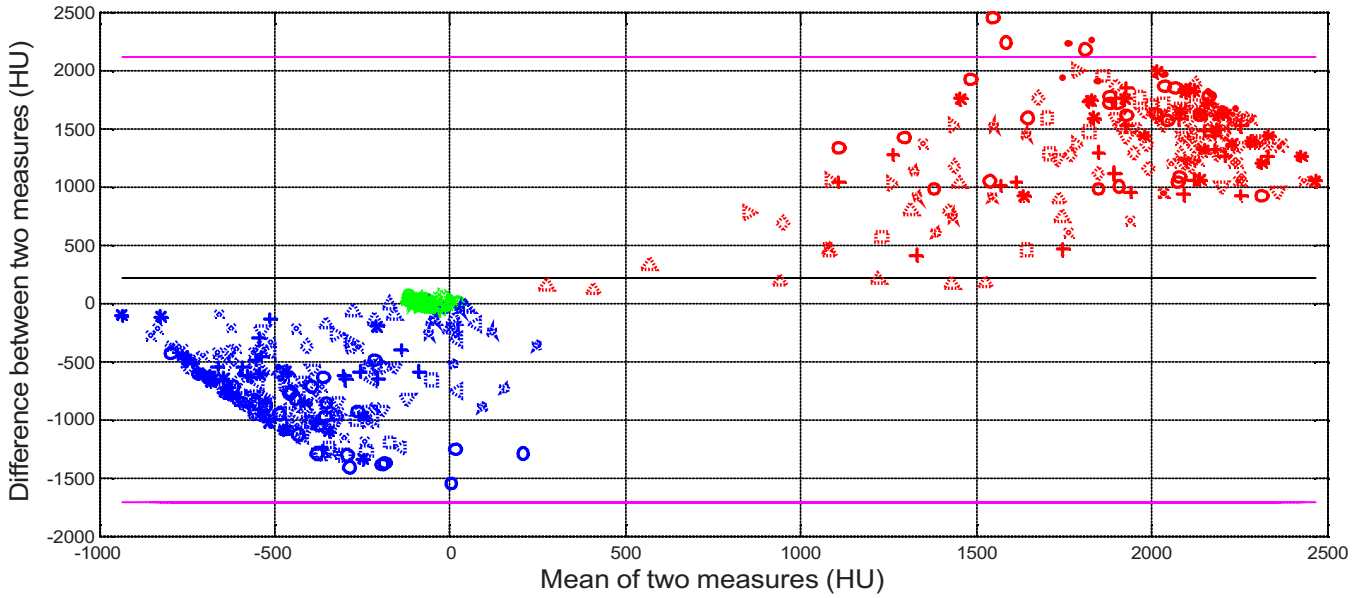

FIG. 6. Bland and Altman plot generated from uncorrected and corrected CT images of 12 clinical studies. The markers on the right side (red online) show the differences (in terms of HU) between uncorrected and corrected images in the overestimated regions, the markers on the left side (blue online) show the differences in underestimated regions, whereas the markers in the middle (green online) show those corresponding to unaffected regions. The data obtained from image slices associated with each patient are demonstrated by a specific marker shape.

tion of the neighboring column of the sinogram matrix is not irrelevant since an adjacent column represents the projections obtained from two slightly different angular positions of the x-ray tube involving contributions from approximately the same tissues. This last step can be exploited for reducing the discontinuity of the interpolated sinogram bins. Optimization of these weighting factors using the GA resulted in an expected combination of values (Table I). The interpolated bins (β) have the major proportion since these are the most relevant values which can be assigned to the corrected sinogram. Also the minor proportion of the neighboring columns (γ) was expected since these bins are only incorporated to decrease the discontinuities along the second dimension of the sinogram matrix. The undesired differences and discon-

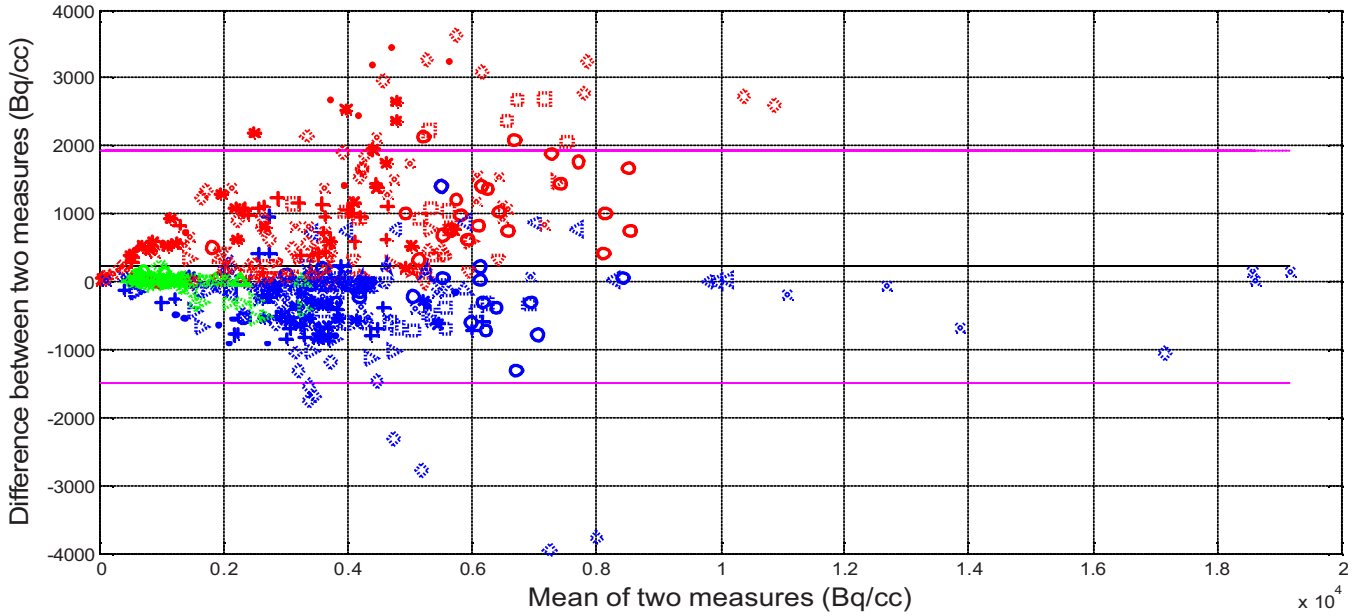

FIG. 7. Bland and Altman plot generated from uncorrected and corrected PET images of 12 clinical studies. The markers in the upper part (red online) show the differences (in Bq/cc) between uncorrected and corrected images in the overestimated regions, the markers in the lower part (blue online) show the differences in underestimated regions, whereas markers in the middle (green online) show those corresponding to unaffected regions. The data obtained from image slices associated with each patient are demonstrated by a specific marker shape.

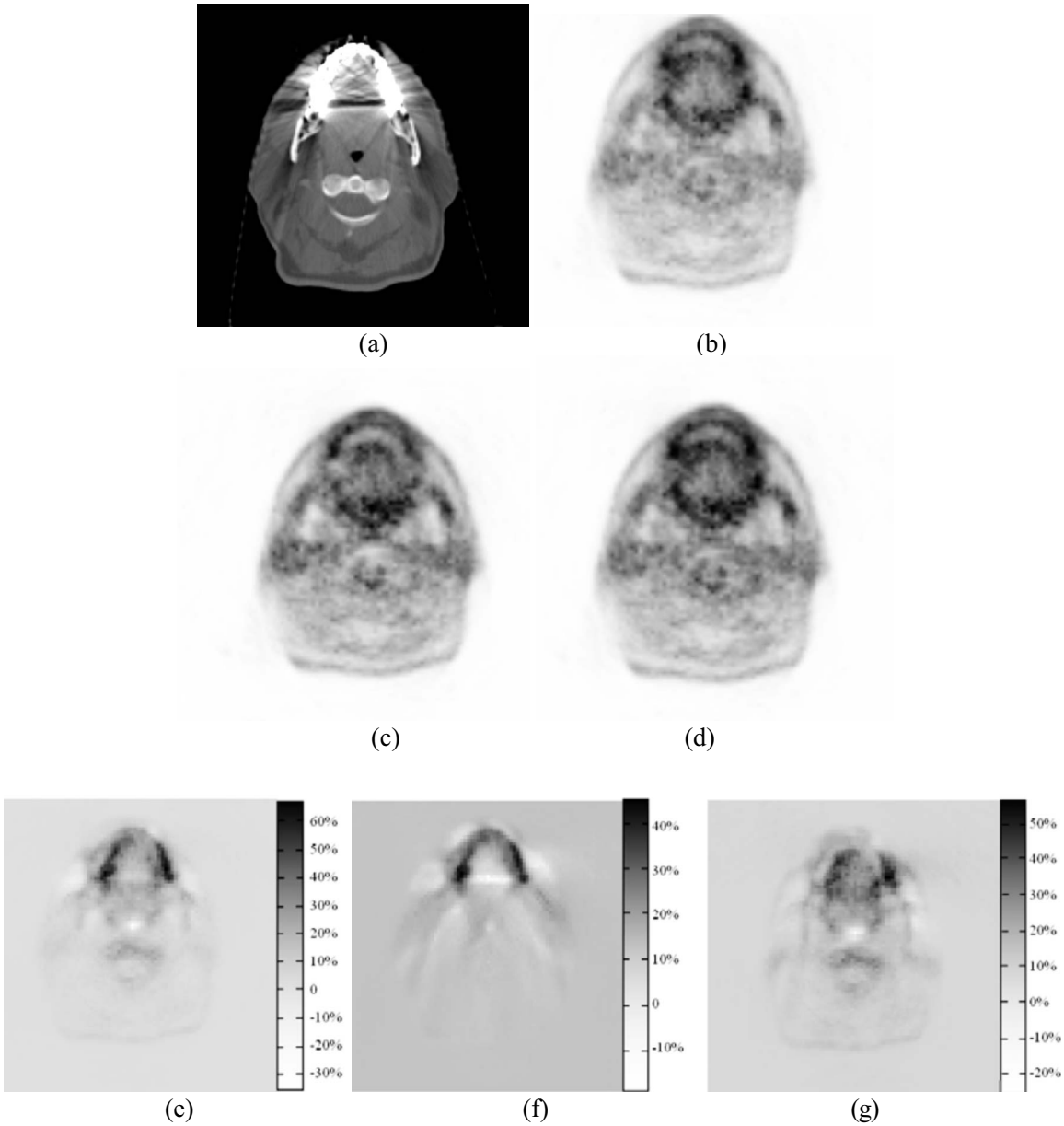

FIG. 8. First clinical PET/CT study used for comparison between the developed MAR algorithm and the method proposed by Hamill *et al.* (Ref. 16). The original CT image (a), corresponding PET images reconstructed using uncorrected CT images (b), using MAR corrected CT images by Hamill *et al.* (Ref. 16) (c), and using MAR corrected CT images using the proposed algorithm (d). (e) Subtraction of images shown in (b) and (c). (f) Subtraction of images shown in (b) and (d). (g) Subtraction of images shown in (c) and (d).

tinuities in the sinogram are reduced to an acceptable degree following application of the optimal combination of weighting factors (Fig. 3). This effect is better shown in the focused part of Figs. 3(b) and 3(c).

The results of clinical head and neck PET/CT data sets demonstrate that the proposed MAR approach is appropriate for generation of reliable μmaps which result in more accurate attenuation correction of PET data. The Bland and Altman plots generated from uncorrected and corrected CT data (Fig. 6) clearly show the potential of the proposed MAR algorithm for elimination of over- and/or underestimations of HUs caused by metallic artifacts. The red markers reflecting the difference between tracer uptake in the overestimated regions in the original CT images and the corresponding regions in the corrected CT images are always in the positive part of the plot, thus corroborating the hypothesis that the proposed MAR approach reduces the overestimation of attenuation coefficients. Likewise, the blue markers reflecting the underestimated regions are situated in the negative part of the plot substantiating the potential of the method to correct for the underestimations. In the unaffected regions (green markers) the differences are around zero, as expected.

Figure 7 illustrates the corresponding results for the attenuation corrected PET data. The same observations can be made for this plot, except for few regions corresponding to underestimated regions of CT images, which confirms the capability of the proposed MAR algorithm to reduce over- and/or underestimation of tracer uptake. Further validation of

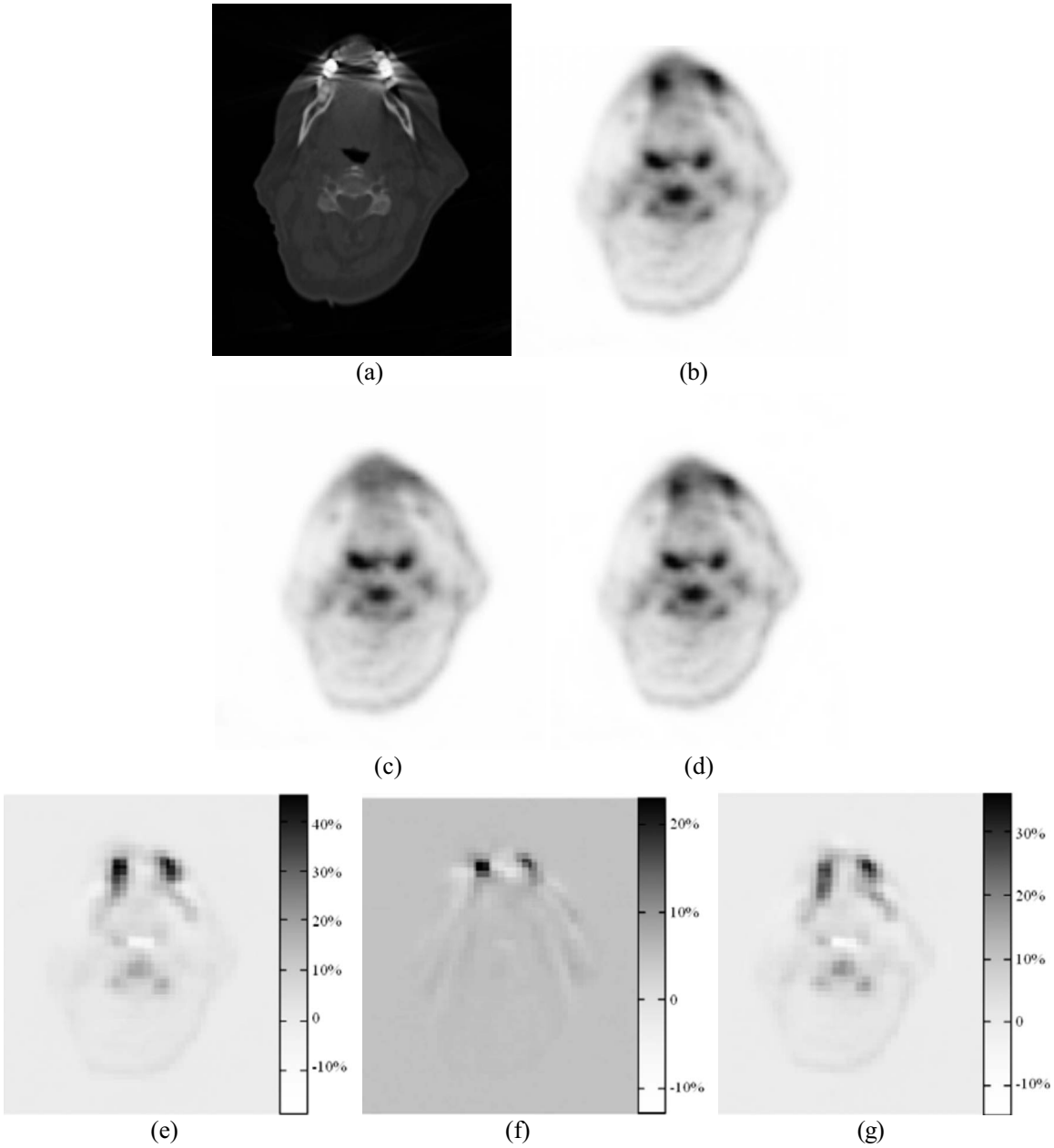

FIG. 9. Second clinical PET/CT study used for comparison between the developed MAR algorithm and the method proposed by Hamill *et al.* (Ref. 16). The original CT image (a), corresponding PET images reconstructed using uncorrected CT images (b), using MAR corrected CT images by Hamill *et al.* (Ref. 16) (c), and using MAR corrected CT images using the proposed algorithm (d). (e) Subtraction of images shown in (b) and (c). (f) Subtraction of images shown in (b) and (d). (g) Subtraction of images shown in (c) and (d).

the MAR approach was performed using the RWT method. In this method, the FOM is defined in such a way that the technique which results in the lowest value of the FOM can be considered as the one producing the most similar results to the assumed gold standard. This is due to the fact that the lowest FOM refers to the smallest error [Eq. (4)]. The FOM calculated for the corrected PET data using the proposed MAR algorithm is less than the one obtained from the uncorrected data, suggesting that using the proposed method produces more reliable results.

The proposed algorithm was compared with the one proposed by Hamill *et al.*[16] and implemented on commercial software supplied by Siemens (Figs. 8 and 9). Although both methods decrease the over- and underestimating artifacts, the results obtained using the method by Hamill *et al.*[16] cause larger modifications of the activity concentrations compared to the proposed MAR algorithm. Since the ground truth is not available for comparison, a reliable judgment of the performance of both algorithms in clinical setting is challenging. Notwithstanding, Figs. 8(e) and 8(f) and Figs. 9(e) and 9(f) indicate that the proposed method has followed the artifact patterns in the correction procedure since the high and low values in the subtracted image match more closely the artifactual regions in the corresponding CT images.

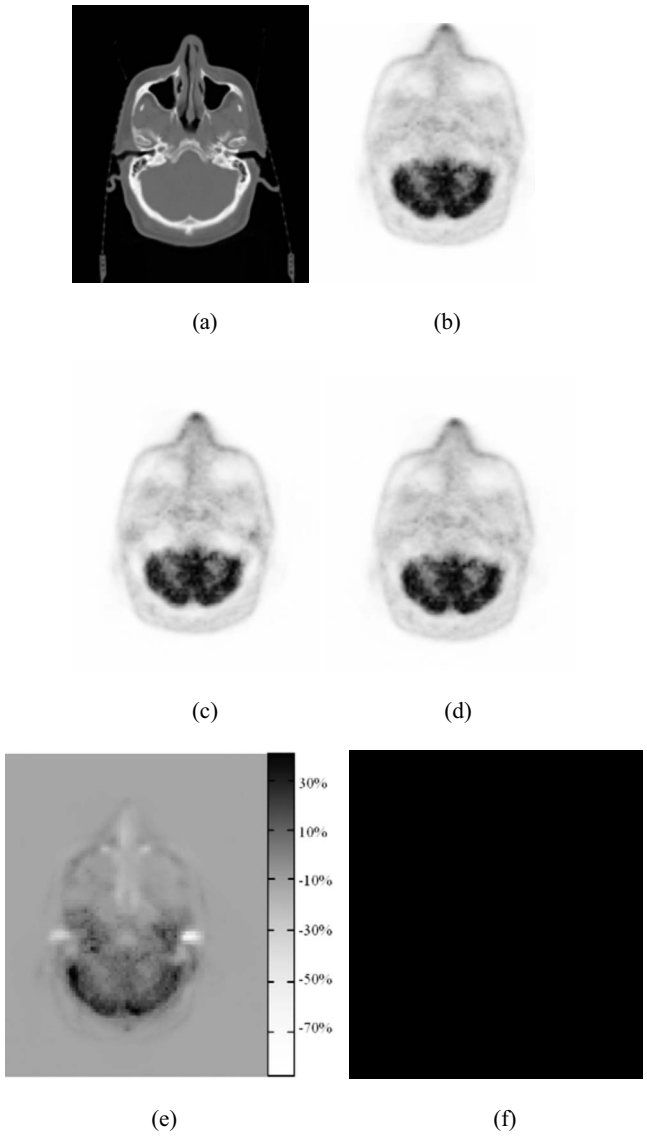

FIG. 10. Comparison between the developed MAR algorithm and the method proposed by Hamill *et al.* (Ref. 16) in regions free of metallic artifacts. The original CT image (a), corresponding PET images reconstructed using uncorrected CT images (b), using MAR corrected CT images by Hamill *et al.* (Ref. 16) (c), and using MAR corrected CT images using the proposed algorithm (d). (e) Subtraction of images shown in (b) and (c). (f) Subtraction of images shown in (b) and (d).

Among the physicians' expectations from a MAR algorithm is that it should not influence the slices that do not include metallic implants and as such are not affected by metallic artifacts. Figure 10 shows how the two algorithms handle artifact-free images. Since the starting point of the proposed algorithm uses the highest HU value in the CT image, it does not modify the slices that do not contain metallic artifacts. On the contrary, the method proposed by Hamill *et al.*[16] processes all slices which can cause over- and/or underestimation of tracer uptake in metal artifact-free regions. As shown in Fig. 10(e), application of the latter method resulted in a considerable decrease of FDG uptake in the brain which might lead to inaccurate interpretation of the images.

V. CONCLUSION

Improvement of the novel MAR algorithm to correct for dental metallic artifacts using optimized weighting factors leads to an approximately smooth and continuous sinogram which results in more reliable correction for metallic artifacts in regions adjacent to metallic objects. This approach allowed the reduction of over- and/or underestimation of tracer uptake in CT-based attenuation corrected PET images of head and neck patients, and as such, the achievement of more accurate quantitative analysis.

ACKNOWLEDGMENTS

This work was supported by Tehran University of Medical Sciences under Grant No. 6932, the Swiss National Science Foundation under Grant No. 3152A0-102143, and a research grant from Siemens Healthcare.

[a]Author to whom correspondence should be addressed. Habib Zaidi, Ph.D Division of Nuclear Medicine, Geneva University Hospital, CH-1211 Geneva, Switzerland. Electronic mail: habib.zaidi@hcuge.ch; Telephone: +41 22 372 7258. Fax: +41 22 372 7169.

[1]D. W. Townsend, "Multimodality imaging of structure and function," Phys. Med. Biol. **53**, R1–R39 (2008).
[2]J. H. Kim, J. Czernin, M. S. Allen-Auerbach, B. S. Halpern, B. J. Fueger, J. R. Hecht, O. Ratib, M. E. Phelps, and W. A. Weber, "Comparison between 18F-FDG PET, in-line PET/CT, and software fusion for restaging of recurrent colorectal cancer," J. Nucl. Med. **46**, 587–595 (2005).
[3]H. Zaidi, M. L. Montandon, and A. Alavi, "Advances in attenuation correction techniques in PET," PET Clin. **2**, 191–217 (2007).
[4]A. Alessio, P. Kinahan, K. Champley, and J. Caldwell, "Attenuation-emission alignment in cardiac PET/CT based on consistency conditions," Med. Phys. **37**, 1191–1200 (2010).
[5]G. W. Goerres, T. F. Hany, E. Kamel, G. K. von Schulthess, and A. Buck, "Head and neck imaging with PET and PET/CT: Artefacts from dental metallic implants," Eur. J. Nucl. Med. Mol. Imaging **29**, 367–370 (2002).
[6]E. M. Kamel, C. Burger, A. Buck, G. K. von Schulthess, and G. W. Goerres, "Impact of metallic dental implants on CT-based attenuation correction in a combined PET/CT scanner," Eur. Radiol. **13**, 724–728 (2003).
[7]C. Lemmens, M. L. Montandon, J. Nuyts, O. Ratib, P. Dupont, and H. Zaidi, "Impact of metal artefacts due to EEG electrodes in brain PET/CT imaging," Phys. Med. Biol. **53**, 4417–4429 (2008).
[8]C. Nahmias, C. Lemmens, D. Faul, E. Carlson, M. Long, T. Blodgett, J. Nuyts, and D. Townsend, "Does reducing CT artifacts from dental implants influence the PET interpretation in PET/CT studies of oral cancer and head and neck cancer?" J. Nucl. Med. **49**, 1047–1052 (2008).
[9]W. A. Kalender, R. Hebel, and J. Ebersberger, "Reduction of CT artifacts caused by metallic implants," Radiology **164**, 576–577 (1987).
[10]M. Yazdia, L. Gingras, and L. Beaulieu, "An adaptive approach to metal artifact reduction in helical computed tomography for radiation therapy treatment planning: experimental and clinical studies," Int. J. Radiat. Oncol., Biol., Phys. **62**, 1224–1231 (2005).
[11]M. Bazalova, L. Beaulieu, S. Palefsky, and F. Verhaegen, "Correction of CT artifacts and its influence on Monte Carlo dose calculations," Med. Phys. **34**, 2119–2132 (2007).
[12]M. Yazdi and L. Beaulieu, "A novel approach for reducing metal artifacts due to metallic dental implants," in *IEEE Nuclear Science Symposium Conference Record*, San Diego, 2006, pp. 2260–2263.
[13]G. Wang, D. L. Snyder, J. A. O'Sullivan, and M. W. Vannier, "Iterative deblurring for CT metal artifact reduction," IEEE Trans. Med. Imaging **15**, 657–664 (1996).
[14]S. Zhao, D. Robertson, G. Wang, and B. Whiting, "X-ray ct metal artifact reduction using wavelets: An application for imaging total hip prostheses," IEEE Trans. Med. Imaging **19**, 1238–1247 (2000).
[15]S. Zhao, K. T. Bae, B. Whiting, and G. Wang, "A wavelet method for metal artifact reduction with multiple metallic objects in the field of view," J. X-Ray Sci. Technol. **10**, 67–76 (2002).

[16]J. J. Hamill, R. C. Brunken, B. Bybel, F. P. DiFilippo, and D. D. Faul, "A knowledge-based method for reducing attenuation artefacts caused by cardiac appliances in myocardial PET/CT," Phys. Med. Biol. **51**, 2901–2918 (2006).
[17]S. Mirzaei, M. Guerchaft, C. Bonnier, P. Knoll, M. Doat, and P. Braeutigam, "Use of segmented CT transmission map to avoid metal artifacts in PET images by a PET-CT device," BMC Nucl. Med. **5**, 3 (2005).
[18]J. A. Kennedy, O. Israel, A. Frenkel, R. Bar-Shalom, and H. Azhari, "The reduction of artifacts due to metal hip implants in CT-attenuation corrected PET images from hybrid PET/CT scanners," Med. Biol. Eng. Comput. **45**, 553–562 (2007).
[19]C. Lemmens, D. Faul, and J. Nuyts, "Suppression of metal artifacts in CT using a reconstruction procedure that combines MAP and projection completion," IEEE Trans. Med. Imaging **28**, 250–260 (2009).
[20]M. Abdoli, M. R. Ay, A. Ahmadian, and H. Zaidi, "A virtual sinogram method to reduce dental metallic implant artefacts in computed tomography-based attenuation correction for PET," Nucl. Med. Commun. **31**, 22–31 (2010).
[21]D. Kincaid and W. Cheney, *Numerical Analysis: Mathematics of Scientific Computing*, 3rd ed. (Brooks/Cole Publishing Company, Boston, 2002).
[22]M. Abdoli, M. R. Ay, A. Ahmadian, and H. Zaidi, "Reduction of dental filling metallic artifacts in CT-based attenuation correction of PET data using weighted virtual sinograms," in *IEEE Nuclear Science Symposium Conference Record*, Orlando, 2009, pp. 2752–2755.
[23]M. Mitchell, *Introduction to Genetic Algorithms* (MIT Press, Cambridge, MA, 1996).
[24]J. W. Hoppin, M. A. Kupinski, G. A. Kastis, E. Clarkson, and H. H. Barret, "Objective comparison of quantitative imaging modalities without the use of a gold standard," IEEE Trans. Med. Imaging **21**, 441–449 (2002).